

# Genetic Correction of a LRRK2 Mutation in Human iPSCs Links Parkinsonian Neurodegeneration to ERK-Dependent Changes in Gene Expression

Peter Reinhardt,<sup>1,10</sup> Benjamin Schmid,<sup>2,10</sup> Lena F. Burbulla,<sup>2</sup> David C. Schöndorf,<sup>2,4</sup> Lydia Wagner,<sup>1</sup> Michael Glatza,<sup>1</sup> Susanne Höing,<sup>1</sup> Gunnar Hargus,<sup>1,4</sup> Susanna A. Heck,<sup>2</sup> Ashutosh Dhingra,<sup>2,5</sup> Guangming Wu,<sup>1</sup> Stephan Müller,<sup>3</sup> Kathrin Brockmann,<sup>2</sup> Torsten Kluba,<sup>6</sup> Martina Maisel,<sup>2</sup> Rejko Krüger,<sup>2</sup> Daniela Berg,<sup>2</sup> Yaroslav Tsytsyura,<sup>7</sup> Cora S. Thiel,<sup>7</sup> Olympia-Ekaterini Psathaki,<sup>1</sup> Jürgen Klingauf,<sup>7</sup> Tanja Kuhlmann,<sup>4</sup> Marlene Klewin,<sup>8</sup> Heiko Müller,<sup>8</sup> Thomas Gasser,<sup>2,\*</sup> Hans R. Schöler,<sup>1,9,\*</sup> and Jared Sternecker<sup>1</sup>

<sup>1</sup>Department of Cell and Developmental Biology, Max Planck Institute for Molecular Biomedicine, Röntgenstrasse 20, 48149 Münster, Germany

<sup>2</sup>Department of Neurodegenerative Diseases

<sup>3</sup>Department of Epileptology

Hertie Institute for Clinical Brain Research, University of Tübingen, and German Center for Neurodegenerative Diseases, 72076 Tübingen, Germany

<sup>4</sup>Institute of Neuropathology, University Hospital Münster, Albert-Schweitzer-Campus 1, Gebäude A7, 48149 Münster, Germany

<sup>5</sup>Graduate School of Cellular & Molecular Neuroscience

<sup>6</sup>Department of Orthopaedic Surgery

University of Tübingen, 72076 Tübingen, Germany

<sup>7</sup>Cellular Biophysics Group, Institute for Medical Physics and Biophysics, Westfälische Wilhelms-Universität Münster, Robert-Koch Str. 31, 48149 Münster, Germany

<sup>8</sup>Department of Pharmacology, Lead-Discovery-Center GmbH, Otto-Hahn-Strasse 15, 44227 Dortmund, Germany

<sup>9</sup>Medical Faculty, University of Münster, Domagkstrasse 3, 48149 Münster, Germany

<sup>10</sup>These authors contributed equally and share first authorship

\*Correspondence: [thomas.gasser@uni-tuebingen.de](mailto:thomas.gasser@uni-tuebingen.de) (T.G.), [office@mpi-muenster.mpg.de](mailto:office@mpi-muenster.mpg.de) (H.R.S.)

<http://dx.doi.org/10.1016/j.stem.2013.01.008>

## SUMMARY

The *LRRK2* mutation G2019S is the most common genetic cause of Parkinson's disease (PD). To better understand the link between mutant *LRRK2* and PD pathology, we derived induced pluripotent stem cells from PD patients harboring *LRRK2* G2019S and then specifically corrected the mutant *LRRK2* allele. We demonstrate that gene correction resulted in phenotypic rescue in differentiated neurons and uncovered expression changes associated with *LRRK2* G2019S. We found that *LRRK2* G2019S induced dysregulation of *CPNE8*, *MAP7*, *UHRF2*, *ANXA1*, and *CADPS2*. Knockdown experiments demonstrated that four of these genes contribute to dopaminergic neurodegeneration. *LRRK2* G2019S induced increased extracellular-signal-regulated kinase 1/2 (ERK) phosphorylation. Transcriptional dysregulation of *CADPS2*, *CPNE8*, and *UHRF2* was dependent on ERK activity. We show that multiple PD-associated phenotypes were ameliorated by inhibition of ERK. Therefore, our results provide mechanistic insight into the pathogenesis induced by mutant *LRRK2* and pointers for the development of potential new therapeutics.

## INTRODUCTION

Parkinson's disease (PD) is the second most common neurodegenerative disease worldwide and affects an estimated 1 in 1,000 people in Europe (European Brain Council, 2011). Although most cases of PD are sporadic, about 5%–10% of patients have familial PD (fPD) following an autosomal-recessive or -dominant inheritance pattern (Schiesling et al., 2008). These two inheritance forms appear to have different pathologies (Schiesling et al., 2008). Unlike patients with autosomal-recessive fPD, patients with autosomal-dominant fPD typically show extensive formation of Lewy bodies in different parts of the brain. Alpha-synuclein ( $\alpha$ SYN), the protein encoded by the gene *SNCA*, is the major component of Lewy bodies, indicating that  $\alpha$ SYN plays a central role in the pathogenesis of PD (Spillantini et al., 1997). *SNCA* was the first gene identified as being mutated in patients with fPD (Polymeropoulos et al., 1997).

In 2004, two research groups simultaneously discovered mutations in the *Leucine-rich repeat kinase 2* (*LRRK2*) gene in patients with fPD (Paisán-Ruiz et al., 2004; Zimprich et al., 2004). Like *SNCA* mutations, *LRRK2* mutations result in autosomal-dominant fPD. Mutations in *LRRK2* have been found in about 2% of patients with sporadic PD (Berg et al., 2005), with much higher prevalence rates in some populations, e.g., Ashkenazi Jews (Ozelius et al., 2006). Patients with PD with *LRRK2* mutations most often exhibit Lewy body pathology, and experiments in the mouse model have suggested a link between *LRRK2* and *SNCA* (Lin et al., 2009; Ross et al., 2006). G2019S

is the most common mutation of *LRRK2*, and mutations in *LRRK2*, including G2019S, have been suggested to lead to increased expression of *SNCA* (Carballo-Carbajal et al., 2010; Nguyen et al., 2011). Therefore, *LRRK2* mutations are thought to confer susceptibility to PD through *SNCA* (Cookson, 2010). However, it should be noted that although most patients with PD harboring *LRRK2* mutations manifest alpha-synucleinopathy, patients with nigral degeneration without  $\alpha$ SYN aggregation have been reported (Cookson et al., 2008).

Several lines of evidence suggest a role for TAU in PD pathology. Genome-wide association studies have demonstrated that polymorphisms at the *Microtubule-associated protein TAU (MAPT)* locus, which encodes TAU, are associated with PD. In addition, it has been shown that the *MAPT* haplotype influences age at onset in *LRRK2* mutation carriers (Golub et al., 2009), and there has been at least one documented case of a *LRRK2* G2019S carrier having TAU pathology (Rajput et al., 2006). Interestingly, it has been suggested that TAU may colocalize with  $\alpha$ SYN in a subset of Lewy bodies (Ishizawa et al., 2003).

Human induced pluripotent stem cell (hiPSC) technology offers a unique opportunity to study the mechanism of PD pathogenesis induced by *LRRK2* G2019S, which could enable the development of new therapies. In 2006, Shinya Yamanaka demonstrated that expression of four genes in fibroblasts induced the formation of pluripotent stem cells, with the same self-renewal and differentiation potential as embryonic stem cells (Takahashi and Yamanaka, 2006). Nguyen et al. (2011) first demonstrated that this technology could be used to generate iPSC lines from patients with PD harboring *LRRK2* G2019S. It was reported that differentiated midbrain dopaminergic (mDA) neurons, which are preferentially lost in patients with PD, were more susceptible to oxidative stress and had increased levels of  $\alpha$ SYN. Subsequently, Sánchez-Danés et al. (2012) showed increased  $\alpha$ SYN and aberrant autophagy in mDA neurons differentiated from iPSC lines of PD patients with and without *LRRK2* G2019S. However, PD phenotypes are affected by polymorphisms at multiple loci. For example, patients with *LRRK2* mutations will exhibit variable phenotypes when additional polymorphisms are present in either *SNCA* or *MAPT* (Botta-Orfila et al., 2012; Golub et al., 2009). As a result, it is unclear whether these observed phenotypes in iPSC-derived neurons were specifically due to *LRRK2* G2019S. Because of the large variability in the genetic background between individuals, it is very difficult to detect and study molecular changes resulting from a specific allele such as *LRRK2* G2019S.

Gene correction of iPSCs from patients with known genetic mutations is a powerful tool for overcoming this limitation of the use of iPSCs. Here, we report mechanistic insights for mDA neurodegeneration induced by *LRRK2* G2019S by using cultures of mDA neurons differentiated from isogenic iPSC lines. We show that targeted correction of *LRRK2* G2019S ameliorated a deficit in neurite outgrowth and a defect in basal autophagy and increased  $\alpha$ SYN, TAU, and susceptibility to oxidative stress. In addition, we demonstrate that targeted insertion of *LRRK2* G2019S into iPSCs from a healthy donor was sufficient to recapitulate the disease phenotypes. With isogenic cultures, we were able to detect dysregulation of *Copine VIII (CPNE8)*, *Annexin A1 (ANXA1)*, *Microtubule-associated protein 7 (MAP7)*,

*Calcium-dependent activator protein for secretion 2 (CADPS2)*, and *Ubiquitin-like with PHD and ring finger domains 2 (UHRF2)*, which are involved in other neurodegenerative pathologies but have not previously been associated with PD. Pharmacological inhibition of *LRRK2* kinase activity corrected these gene expression changes and rescued PD-associated phenotypes. Knock-down experiments demonstrated that dysregulation of four of these genes significantly contributed to mDA neurodegeneration under oxidative stress. Finally, we demonstrate that *LRRK2* G2019S was associated with increased activation of ERK and that inhibition of ERK ameliorated mDA neurodegeneration, neurite outgrowth, and the dysregulation of *CADPS2*, *CPNE8*, and *UHRF2*. Therefore, these results reveal molecular details for the pathogenesis of mutant *LRRK2* and possible new targets for the development of new therapeutics for patients with PD.

## RESULTS

### Generation and Gene Correction of iPSCs

We derived iPSCs from two patients harboring the *LRRK2* mutation G2019S (Table S1 available online). The samples used in this study were derived from two female patients with PD born in 1958 and 1931 (designated L1 and L2, respectively). As nonisogenic healthy controls, we used iPSC lines derived from four healthy women born in 1959, 1931, 1943, and 1932 (designated C1, C2, C3, and C4, respectively) (Table S1). Dermal fibroblasts from skin punch biopsies of patients with PD or healthy controls were expanded and infected with retroviral expression vectors containing the genes indicated and iPSCs were generated (Takahashi et al., 2007). Individual clonal iPSC lines derived from L1 and L2 were designated L1-1 and L2-1, respectively (Table S1).

Multiple assays were used to confirm the reprogramming of fibroblasts into all the iPSC lines used in this study. Immunostaining demonstrated that the iPSC lines expressed the pluripotent markers NANOG, OCT4, SSEA4, and TRA1-81 (Figures 1A and S1A). Real-time quantitative PCR (qRT-PCR) analysis showed that iPSCs expressed pluripotency markers at levels comparable with human embryonic stem cells (hESCs) (Figures 1B and S1B) and silencing of the retroviral vectors, which is a hallmark of bona fide iPSCs (Figure S1C; Hotta and Ellis, 2008). Pluripotent differentiation potential of each iPSC line was tested in vitro via embryoid body (EB)-mediated differentiation and in vivo via teratoma formation (Figures 1C, 1D, S2A, and S2B). Each line was verified to be euploid via microarray profiling of single-nucleotide polymorphisms.

Genome-wide association studies have revealed that multiple genetic variants are associated with PD (Simón-Sánchez et al., 2009). Therefore, given the variable phenotypes associated with specific *LRRK2* mutations, it is very likely that variants in other genetic loci modify the phenotype induced by *LRRK2* G2019S. To account for this, we gene-corrected iPSC lines from both patients to obtain three isogenic lines per patient that differed only in this mutation. A correction vector was inserted site specifically by cotransfecting it with zinc finger nucleases (ZFNs) designed to introduce a double-strand break adjacent to the G2019S mutation of the *LRRK2* gene. Because *LRRK2* mutations are inherited dominantly, our patients with PD are heterozygous for the G2019S mutation. As such, only

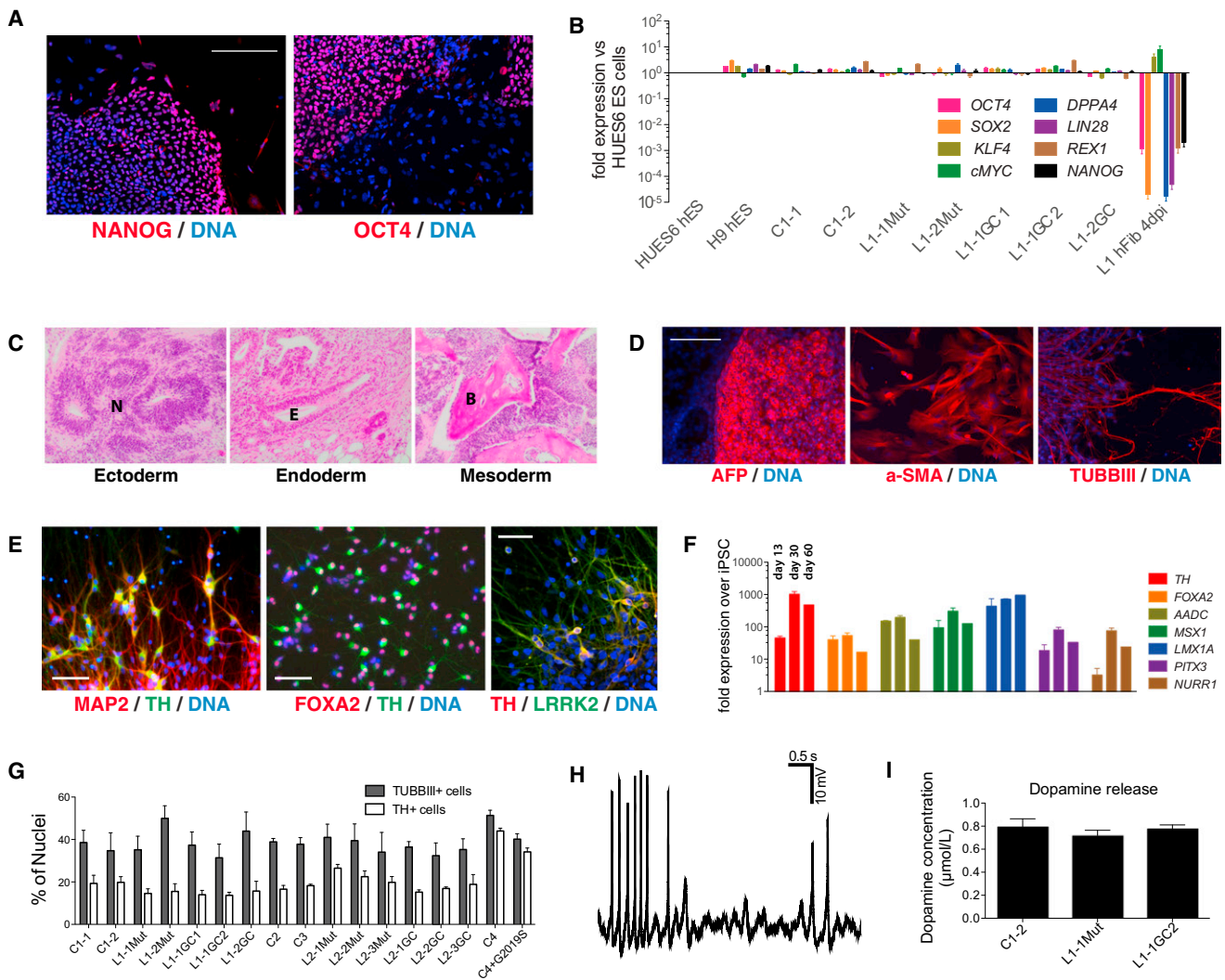


**Figure 1. iPSC Line Derivation and Differentiation into Functional mDA Neurons**

(A) Immunostaining for the indicated markers was performed along with nuclear counterstaining by Hoechst. See also Figure S1A.  
 (B) qRT-PCR analysis of the indicated iPSC lines for the expression of the indicated pluripotency markers relative to HUES6 hESCs. Fibroblasts from patient 1 at 4 days after retroviral infection are also shown. See also Figures S1B and S1C. Error bars give variation from using *GAPDH* and *BACT* as housekeeping genes.  
 (C) Teratomas formed from subcutaneous injection of iPSCs into immunodeficient mice were isolated and stained with hematoxylin and eosin. N, neural rosettes; E, gut-like epithelium; B, bone; M, muscle. See also Figure S2.  
 (D) iPSCs were differentiated in vitro via embryoid bodies and immunostained for AFP (endoderm), alpha-SMA (mesoderm), and TUBBIII (ectoderm). See also Figure S2.  
 (E) The differentiation protocol efficiently produces midbrain dopaminergic neurons, shown by immunostaining for TH, MAP2, and FOXA2. See also Figures S3–S5.  
 (F) qRT-PCR for the indicated markers on the indicated days of differentiation of the iPSC line C3. Error bars show the variation of duplicate experiments. See also Figure S3.  
 (G) Differentiation efficiencies for all lines, given as percentage of cells, identified by nuclei, positive for the indicated marker.  $n = 3-5$  for each line, error bars indicate SEM.  
 (H) Exemplary recording of spontaneous firing of APs in current-clamp mode. See Figure S5 for further characterization.  
 (I) mDA neuron cultures contain mature dopamine-producing neurons, shown by dopamine release upon stimulation of the given lines. Error bars show the variance between two independent differentiation cultures. See also Figures S1–S5 as well as Tables S1 and S2.  
 All scale bars represent 100  $\mu\text{m}$ .

half of the targeted cell lines would be expected to target the correct allele. We used DNA sequencing of iPSCs and differentiated neurons to confirm correction of the G2019S mutation (Figures S2C and S2D). As an additional experimental control, the ZFNs were used to introduce the G2019S mutation into one of the *LRRK2* loci of the control iPSC line C4,

which was derived from a healthy individual. Appropriate expression of the artificially mutated allele was confirmed through quantification by pyro-sequencing with cDNA (Figure S2E). Therefore, through both patient selection and gene targeting, we have a complete set of iPSC lines to study the mechanisms of PD pathogenesis induced by mutant *LRRK2* (Table S1). All

gene-targeted subclones were fully characterized and confirmed to be euploid and pluripotent *in vitro* and *in vivo* (Figures S1 and S2).

### Gene Correction Ameliorates PD-Associated Phenotypes in mDA Neurons

Because PD is characterized by the degeneration of mDA neurons, we directed the differentiation of iPSCs into this neuronal subtype. After 10 days of differentiation, we observed efficient formation of OTX2 and FOXA2 double-positive cells, which are markers of mDA neural progenitors (Figures S3A and S3B). Additional developmental markers associated with the specification of mDA neurons were detected by qRT-PCR after 13, 30, and 60 days of differentiation, including *TH*, *FOXA2*, *AADC*, *MSX1*, *LMX1A*, *PITX3*, and *NURR1* (Figures 1F, S3C, and S3D). Immunostaining demonstrated frequent formation of FOXA2 and TH as well as TH and *LRRK2* double-positive cells (Figures 1E and S4). The efficiency of mDA neuron formation was approximately 20% of the total cells and 50% of all neurons after plating them as single cells on day 30 of differentiation (Figure 1G). Cultures of differentiated mDA neurons stained positively for *NURR1*, which is a marker of mDA neurons, as well as NeuN, MAP2, and SYNAPTOPHYSIN, which are markers of mature neurons (Figures 1E, S5A, and S5B). Analysis of electrophysiology and dopamine release upon chemical stimulation confirmed that the differentiated neurons were functionally mature after 30–35 days of differentiation (Figures 1H, 1I, and S5C–S5G).

Next, we sought to determine whether the gene correction of *LRRK2* G2019S resulted in functional phenotypic correction. Neurite shortening and sensitivity to neurotoxins are phenotypes associated with *LRRK2* G2019S (MacLeod et al., 2006; Nguyen et al., 2011; Sánchez-Danés et al., 2012). We observed a statistically significant ( $p < 0.001$ ) reduction in the velocity of outgrowing neurites harboring *LRRK2* G2019S compared to wild-type controls (Figures 2A–2C). Targeted gene correction of *LRRK2* G2019S rescued this phenotype to a level equal to the wild-type controls (Figures 2A and 2B). Immunostaining showed that about 20% of outgrowing neurites were TH positive, suggesting that this is a general neuronal phenotype and not specific to mDA neurons (Figure 2D).

Previously, Sánchez-Danés et al. (2012), reported that *LRRK2* G2019S was associated with aberrant autophagy in neurons differentiated from iPSCs. Consistent with this report, we found that basal autophagy was significantly reduced by about 20% (Figures S6A and S6B) and increased numbers of autophagosomes were observed in cultures harboring *LRRK2* G2019S (Figures S6C). Similarly, cultures of differentiated mDA neurons were significantly more sensitive to oxidative stress when cultured in N2 medium without the supplement B27 (Figures 3 and 4A), which contains antioxidant proteins such as Catalase and Superoxide Dismutase (Brewer et al., 1993). Addition of the neurotoxins rotenone or 6-hydroxydopamine (6-OHDA) resulted in a small increase in the number of TH and cleaved CASPASE3 double-positive cells in differentiated cultures harboring *LRRK2* G2019S compared to gene-corrected isogenic controls (Figures 3, 4A, 4B, S6D, and S6E). Immunostaining showed that more than 80% of the cells positive for cleaved CASPASE3 also expressed TH (Figure 4C). To further assess

the specificity of neurodegeneration, we differentiated iPSCs into peripheral sensory neurons (Greber et al., 2011), cultured them under conditions of oxidative stress, and immunostained for cleaved CASPASE3 and BRN3A, which mark apoptotic sensory neurons. Compared to mDA neurons, fewer sensory neurons were positive for cleaved CASPASE3, and there was no increase associated with *LRRK2* G2019S (Figure S6F). These results demonstrate that apoptosis was preferentially induced in mDA neurons. In another experiment, we tested whether *LRRK2* G2019S is sufficient to increase sensitivity of mDA neurons to B27 withdrawal and to 6-OHDA- and rotenone-induced toxicity. To do this, we repeated the above assays with neurons derived from the iPSC lines C4 and C4+G2019S, in which we had inserted the G2019S mutation into the *LRRK2* locus of an iPSC line derived from a healthy control. The increase in cytotoxicity was comparable in magnitude with the decrease in cytotoxicity observed after gene correction for mutant *LRRK2* iPSC lines (Figures 3A and 4A). We conclude that mutant *LRRK2* is sufficient to induce increased sensitivity of human mDA neurons to oxidative stress.

To address the question of whether the G2019S mutation results in a gain or loss of function, we repeated the cytotoxicity experiments in the presence of *LRRK2*-IN1, which is a small molecule inhibitor of *LRRK2* kinase activity. We observed a statistically significant increase in mDA neuron survival as measured by cleaved CASPASE3 and TH in the presence of the inhibitor compared to controls (Figures 4D and S6G). A similar trend was observed when cell death was quantified by lactate dehydrogenase (LDH) release (Figures 4E and S6H). These data suggest that *LRRK2* G2019S results in a gain of kinase function, which is consistent with previous reports (Gloeckner et al., 2006; West et al., 2005). Therefore, multiple phenotypic assays confirm that gene correction of *LRRK2* G2019S resulted in functional phenotypic correction.

### *LRRK2* G2019S Causes PD-Associated Changes in TAU and $\alpha$ SYN

Because multiple lines of evidence suggest a role for TAU in PD pathogenesis, we characterized *MAPT* transcription and TAU protein levels. qRT-PCR analysis on triplicate samples on day 30 of differentiation demonstrated that *MAPT* was significantly downregulated by 39% in cultures of mDA neurons containing wild-type *LRRK2* compared with isogenic cultures with G2019S *LRRK2* (Figure 5A). Western blotting confirmed that TAU protein and phospho-Thr181 TAU were significantly lower in cultures of mDA neurons harboring gene-corrected *LRRK2* compared to isogenic cultures with *LRRK2* G2019S (Figures 5B, 5C, and S7A). Immunostaining confirmed that neurons expressing TH were also positive for TAU and phospho-TAU (Figure S7B). These data are consistent with previously published data showing a link between patients with PD, *MAPT*, and *LRRK2*. Interestingly, it has been shown that TAU enhances  $\alpha$ SYN aggregation and toxicity (Badiola et al., 2011). It is also significant to note that increased levels of Thr181-phosphorylated TAU correlate with neurite retraction (Maldonado et al., 2008, 2011), and, as such, could contribute to the neurite outgrowth phenotype in *LRRK2* G2019S neurons.

Because  $\alpha$ SYN pathology is present in most patients with PD harboring mutant *LRRK2*, we assessed the level of *SNCA* mRNA

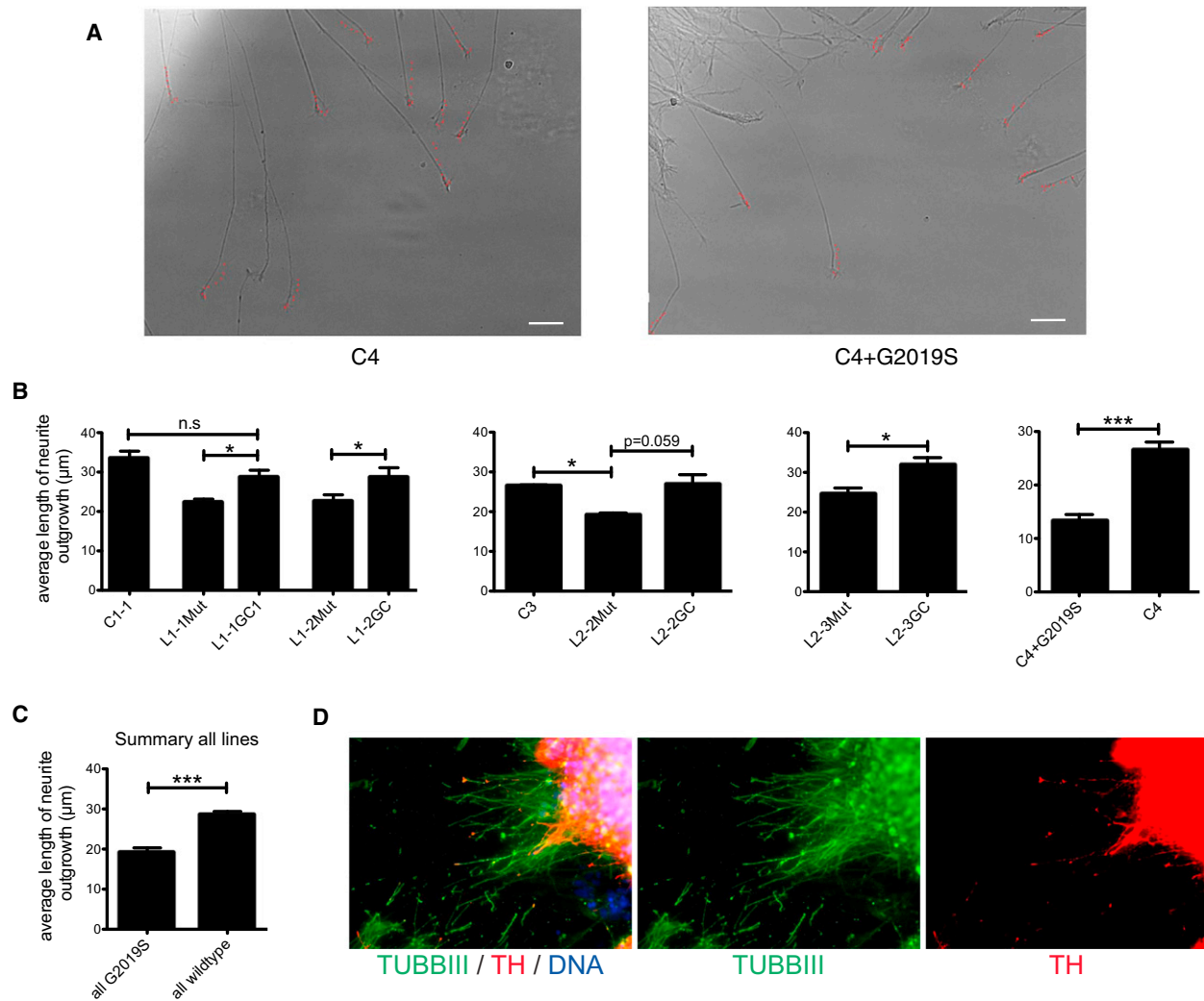


**Figure 2. Gene Correction of *LRRK2* G2019S Ameliorates Neurite Outgrowth Phenotype**

(A) Sample pictures from a neurite outgrowth experiment for neurons differentiated from the indicated isogenic wild-type (left) and G2019S (right) *LRRK2* iPSC line. Red dots indicate the end of the neurite, which was determined every 5 min. Scale bars represent 50 μm.

(B) Individual neurite outgrowth speeds for the indicated lines measured from triplicate cultures, Error bars represent the standard error of the mean (SEM). \* $p < 0.05$ , \*\*\* $p < 0.001$ .

(C) When combined, the results show a significantly lower neurite outgrowth speed in neuron cultures with *LRRK2* G2019S compared to wild-type. Error bars indicate SEM.

(D) The neurite outgrowth reduction is a general neuronal phenotype, as only about 20% of the fastest outgrowing neurons are positive for TH.

and  $\alpha$ SYN protein by mDA neurons that had been differentiated from iPSCs. qRT-PCR showed that isogenic cultures of mDA neurons differentiated for 30 and 60 days expressed comparable levels of *SNCA* (Figure 5D). Immunostaining showed that  $\alpha$ SYN protein in neurons differentiated for 30 days displayed a punctate staining pattern that colocalized with SYNAPTOPHYSIN, which is a marker of mature neurons (Figure S5B). Western blots confirmed the presence of monomeric  $\alpha$ SYN protein in cultures of differentiated mDA neurons (Figure 5E). Because it has been suggested that *LRRK2* G2019S results in increased levels of  $\alpha$ SYN protein (Nguyen et al., 2011), we quantified the level of  $\alpha$ SYN normalized to GAPDH protein levels (Figure S7A). When we initially compared all cultures of mDA neurons with either

wild-type or G2019S *LRRK2* without taking into account matching lines from gene correction, we found no significant difference in  $\alpha$ SYN protein levels between groups. In contrast, when the data was reanalyzed directly comparing the level of  $\alpha$ SYN present in gene-corrected cultures to the respective isogenic cultures with *LRRK2* G2019S, we found that cultures of mDA neurons harboring gene-corrected *LRRK2* contained about 30% less  $\alpha$ SYN protein, which was statistically significant, compared to cultures differentiated from isogenic G2019S *LRRK2* lines (Figure 5F). This is in agreement with human pathophysiological data, which shows extensive  $\alpha$ SYN pathology in PD patients carrying *LRRK2* G2019S (Schiesling et al., 2008). These results are also in agreement with previously published

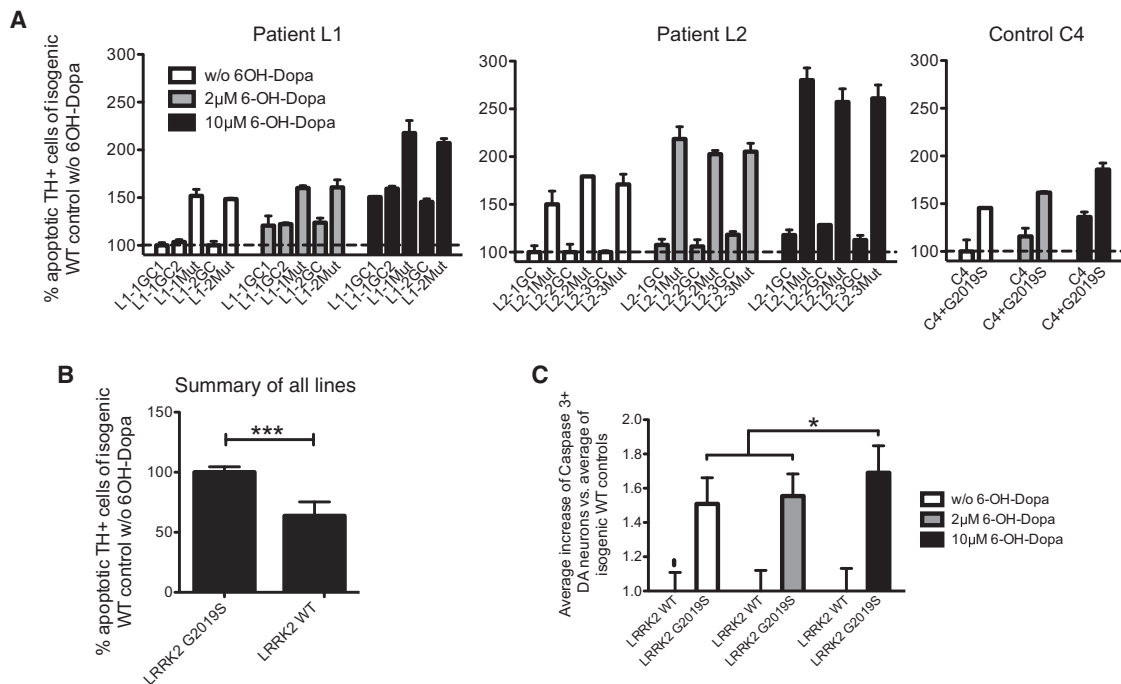


**Figure 3. *LRRK2* G2019S Causes 6-Hydroxydopamine Sensitivity in Human mDA Neurons**

(A) Relative frequency of cleaved CASPASE3 and TH double-positive cells after treating the mDA neurons differentiated from the indicated iPSC line with the indicated concentration of 6-OHDA in N2 medium ( $n = 2$ ). Error bars represent the variation. Data are presented after normalization on the *LRRK2* WT isogenic line that was treated with N2 medium only to correct for basal level of cell death caused by replating and N2 medium alone. For individual primary results, see Figure S6. mDA neurons harboring *LRRK2* G2019S were more susceptible to apoptosis compared to wild-type when cultured only in N2 medium. The magnitude of the difference increased when 6-OHDA was added.

(B) All results together, after normalization by setting all mutant *LRRK2* cultures to 100, show that *LRRK2* G2019S causes a higher sensitivity to cytotoxic stress when comparing mutant to their isogenic wild-type samples. Error bars show the standard deviation. \*\*\* $p < 0.001$  according to t test.

(C) Treatment with 10  $\mu$ M 6-OHDA leads to a faster increase of cell death in *LRRK2* G2019S DA neurons, compared to the isogenic *LRRK2* WT controls. \* $p < 0.05$ , according to the t test. Error bars indicate SEM.

results (Nguyen et al., 2011; Sánchez-Danés et al., 2012). However, we found that the difference in the level of  $\alpha$ SYN was not significant when comparing nonisogenic cultures because of the high variation within the “healthy” neurons. This suggests that the increase in  $\alpha$ SYN protein levels induced by *LRRK2* G2019S cannot reliably be distinguished from the variance already present in our cultures from patients without PD.

### Gene Correction Enables Identification of Novel Genes Dysregulated by *LRRK2* G2019S

To identify possible changes in gene expression caused by *LRRK2* G2019S, we compared the global gene expression profile of cultures after 30 days of differentiation. Three independent hiPSC lines harboring *LRRK2* G2019S were differentiated alongside their isogenic gene-corrected hiPSC lines. In addition, two hiPSC lines derived from age- and sex-matched control patients were differentiated. RNA was harvested and analyzed with Illumina gene expression microarray on day 30 of differentiation. The cluster dendrogram demonstrated that the gene expression profiles of cultures differentiated from a hiPSC line with *LRRK2* G2019S was most closely related to its isogenic gene-corrected culture in each of the three cases (Figure 6A). In addition, we found that cultures of mDA neurons differentiated from the healthy control hiPSC line C1-1 clustered more closely

to cultures differentiated from hiPSC lines derived from patient 2 than to those from patient 1. This was unexpected because the donor for hiPSC line C1-1 was age and gender matched to patient 1. Moreover, the gene expression of cultures differentiated from control line C2, which was derived from a patient age and gender matched to patient 2, was significantly different from all other samples. This clearly shows that derivation of hiPSC lines from patients that are age and gender matched does not result in closely related gene expression patterns after differentiation even though the overall differentiation efficiencies were comparable between all hiPSC lines. In contrast, gene correction resulted consistently in extremely similar expression patterns with the isogenic *LRRK2* G2019S hiPSC line after differentiation. Given the large effect of genetic background on gene expression, our data suggest that it is possible to detect changes specifically associated with *LRRK2* G2019S only through gene correction.

To gain further mechanistic insight into the development of *LRRK2*-related phenotypes, we sought to identify genes whose expression levels were changed by the presence of *LRRK2* G2019S. By using our previous global gene expression profiles, we filtered for genes that were expressed at a minimum threshold level and either up- or downregulated by at least 1.2-fold in the same direction in all three cultures of mDA neurons

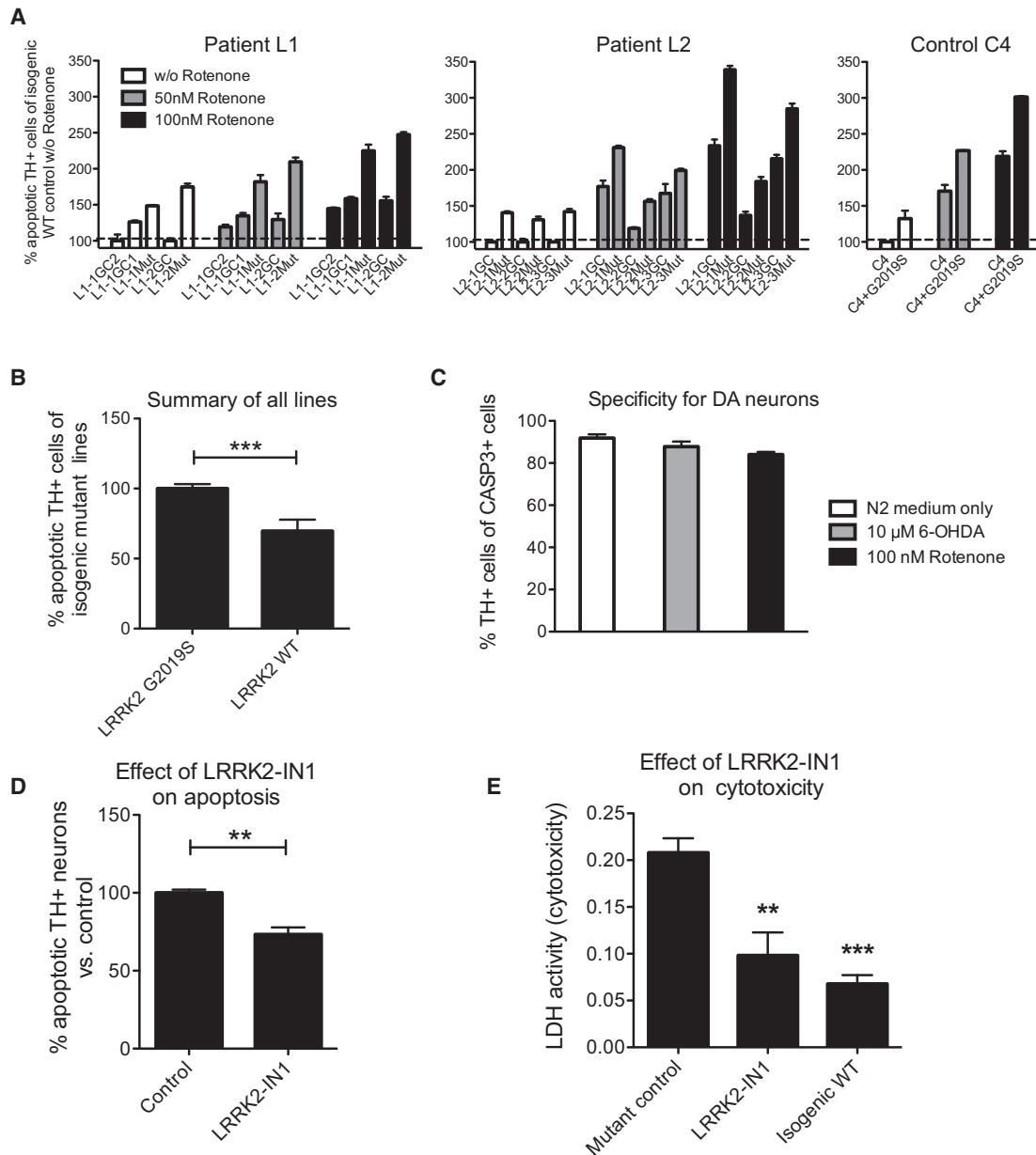


**Figure 4. Gene Correction of *LRRK2* G2019S Ameliorates Sensitivity of Human mDA Neurons to Rotenone**

(A) Relative frequency of cleaved CASPASE3 and TH double-positive cells after treating the mDA neurons of the indicated lines with the indicated concentration of rotenone in N2 medium (n = 2). Error bars represent the variation. Data are normalized to the *LRRK2* WT isogenic line treated with N2 medium alone. mDA neurons harboring *LRRK2* G2019S were more susceptible to apoptosis compared to wild-type when cultured in only N2 medium. The magnitude of the difference increased when rotenone was added.

(B) *LRRK2* G2019S causes a higher sensitivity to cytotoxic stress when compared with the wild-type isogenic line caused by rotenone. Error bars show the standard deviation. These are combined data for isogenic lines L1-1, L1-2, L2-2, L2-3, and C4 at all concentrations used.

(C) Cleaved CASPASE3 was preferentially in cells expressing TH after treatment with the indicated conditions. Error bars indicate variation.

(D and E) 1.5  $\mu$ M LRRK2-IN1, which inhibits LRRK2 kinase activity, rescued mDA neurons from apoptosis. Cultures were differentiated in triplicate from L1-1Mut and C4+G2019S, stressed with 50 nM rotenone, and immunostaining for cleaved CASPASE3 and TH double-positive cells (D) and LDH release (E) compared to DMSO-treated controls. Error bars indicate SEM.

\*\*p < 0.01 and \*\*\*p < 0.001 according to t test. See also Figure S6.

differentiated for 30 days from hiPSCs containing *LRRK2* G2019S compared to gene-corrected *LRRK2*. Subsequently, we differentiated these and additional hiPSC lines in indepen-

dent triplicate cultures for 30 days followed by qRT-PCR validation. Six genes could be corroborated by further samples by qRT-PCR as significantly and consistently dysregulated

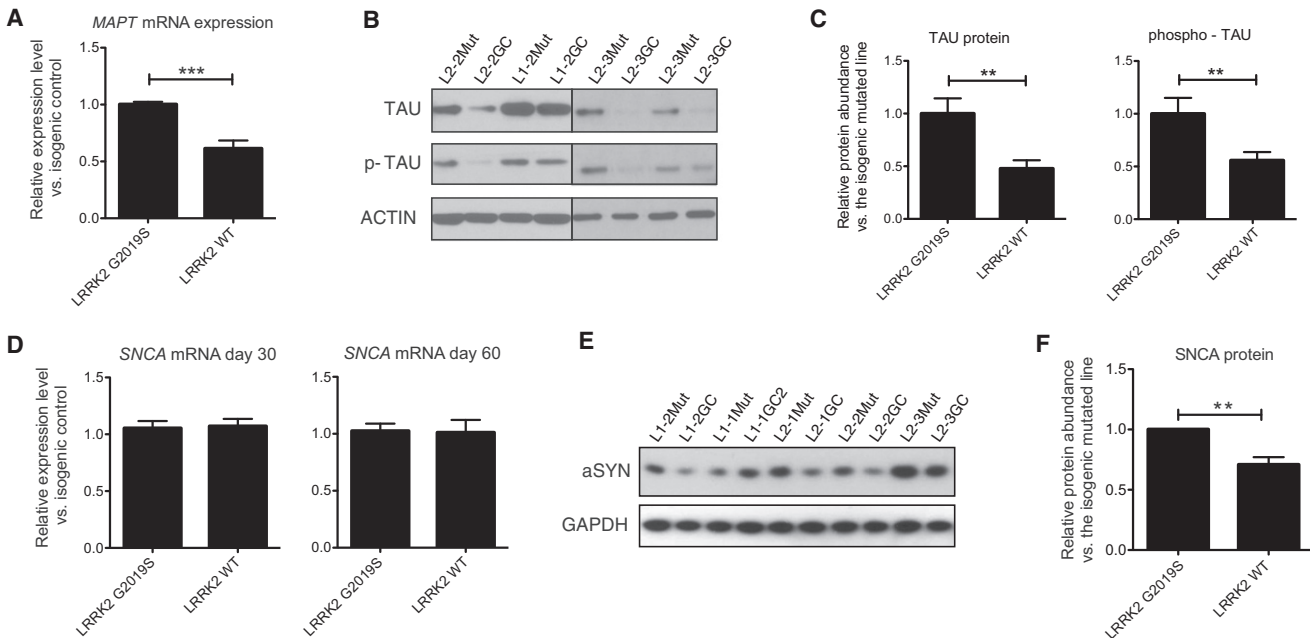


**Figure 5. *LRRK2* G2019S Mutation Leads to Increased Expression of *MAPT* mRNA and TAU Protein as well as Increased  $\alpha$ SYN Protein**

(A) *MAPT* mRNA levels are significantly decreased when comparing triplicate cultures differentiated from *LRRK2* wild-type to isogenic mutant lines.  $n = 6$  lines wild-type,  $n = 5$  mutant, including C4 and C4+G2019S.

(B) Representative western blot results for the given mDA neuron cultures. Independent replicate experiments are shown for lines L2-3Mut and L2-3GC.

(C) Reduced TAU and phospho-TAU (Thr181) protein is found in cultures differentiated from *LRRK2* wild-type compared to isogenic mutant lines. This is an average of individual results shown in Figure S7.

(D) No change in expression is detected by qRT-PCR analysis of *SNCA* expression in mDA neuron cultures differentiated in independent replicate cultures comparing all targeted lines to their isogenic mutant line.  $n = 3-5$  for each line at day 30,  $n = 2-3$  for each line at day 60 of differentiation.

(E) Representative western blot results for the given mDA neuron cultures for  $\alpha$ SYN protein showing lower levels in wild-type compared to isogenic mutant samples.  $\alpha$ SYN protein levels were normalized using GAPDH as a housekeeping gene.

(F) Average  $\alpha$ SYN protein abundance showing a significant decrease in gene-corrected lines compared to their mutant isogenic lines.  $n = 9$ , individual results are shown in Figure S7.

Error bars indicate SEM in all panels. \* $p < 0.05$ , \*\* $p < 0.01$ , \*\*\* $p < 0.001$  according to t test.

by *LRRK2* G2019S in cultures of mDA neurons. The first four that we identified were *CPNE8*, *ANXA1*, *MAP7*, and *CADPS2*, which were downregulated by about 38%, 40%, 30%, and 29%, respectively, in cultures of mDA neurons harboring gene-corrected *LRRK2* compared to isogenic cultures with the G2019S mutation (Figure 6B). In addition, we identified *UHRF2* as significantly upregulated by 16% in cultures of mDA neurons harboring gene-corrected *LRRK2* compared with the isogenic cultures with the G2019S mutation (Figure 6B). To confirm the effect of *LRRK2* G2019S on the expression of these genes, we repeated the experiment with cultures differentiated from the hiPSC line C4, which was derived from a healthy control patient, and from the hiPSC line C4-G2019S, in which the mutation G2019S had been specifically introduced into one endogenous *LRRK2* allele. The results were consistent with the gene-corrected cultures (Figure 6C). Western blotting demonstrated that protein levels of *CPNE8*, *CADPS2*, *ANXA1*, and *MAP7* were significantly altered in cultures with mutant *LRRK2* compared with isogenic controls (Figures 6D and 6E). *UHRF2* was lower in *LRRK2* G2019S samples compared with isogenic controls with a  $p$  value of 0.0533 (Figures 6D and 6E). Inhibition of *LRRK2* kinase activity with *LRRK2*-IN1 rescued the dysregulation of these genes (Figure S6I). Therefore, isogenic cultures

enabled the detection of multiple genes that were specifically dysregulated by *LRRK2* G2019S.

Knockdown experiments were used to assess the contributions of *CPNE8*, *ANXA1*, *MAP7*, *CADPS2*, and *UHRF2* to mDA neurodegeneration under oxidative stress. Cultures of mDA neurons differentiated from iPSC line L1-1Mut were treated with Accell siRNA SMARTpool targeting one of the identified dysregulated genes. qRT-PCR demonstrated that the target gene expression was decreased by 50%–80% (Figure 6F). After exposure to oxidative stress via B27 withdrawal alone or in combination with 50 nM rotenone, neurodegeneration was assessed by LDH release and double-immunostaining for cleaved *CASPASE3* and TH. We found that knockdown of *CPNE8*, *CADPS2*, and *MAP7* resulted in a statistically significant decrease in the number of cleaved *CASPASE3* and TH double-positive neurons (Figures 6G and 6H). In contrast, we found that knockdown of *UHRF2* resulted in small, but significant, increase in the number of cleaved *CASPASE3* and TH double-positive neurons (Figures 6G and 6H). No significant change was observed with the knockdown of *ANXA1* (Figures 6G and 6H). Knockdown of *CPNE8*, *CADPS2*, and *MAP7* was also protective when we used LDH release as a measure of cytotoxicity (Figures S6J and S6K). These results demonstrate that the upregulation of *CPNE8*,

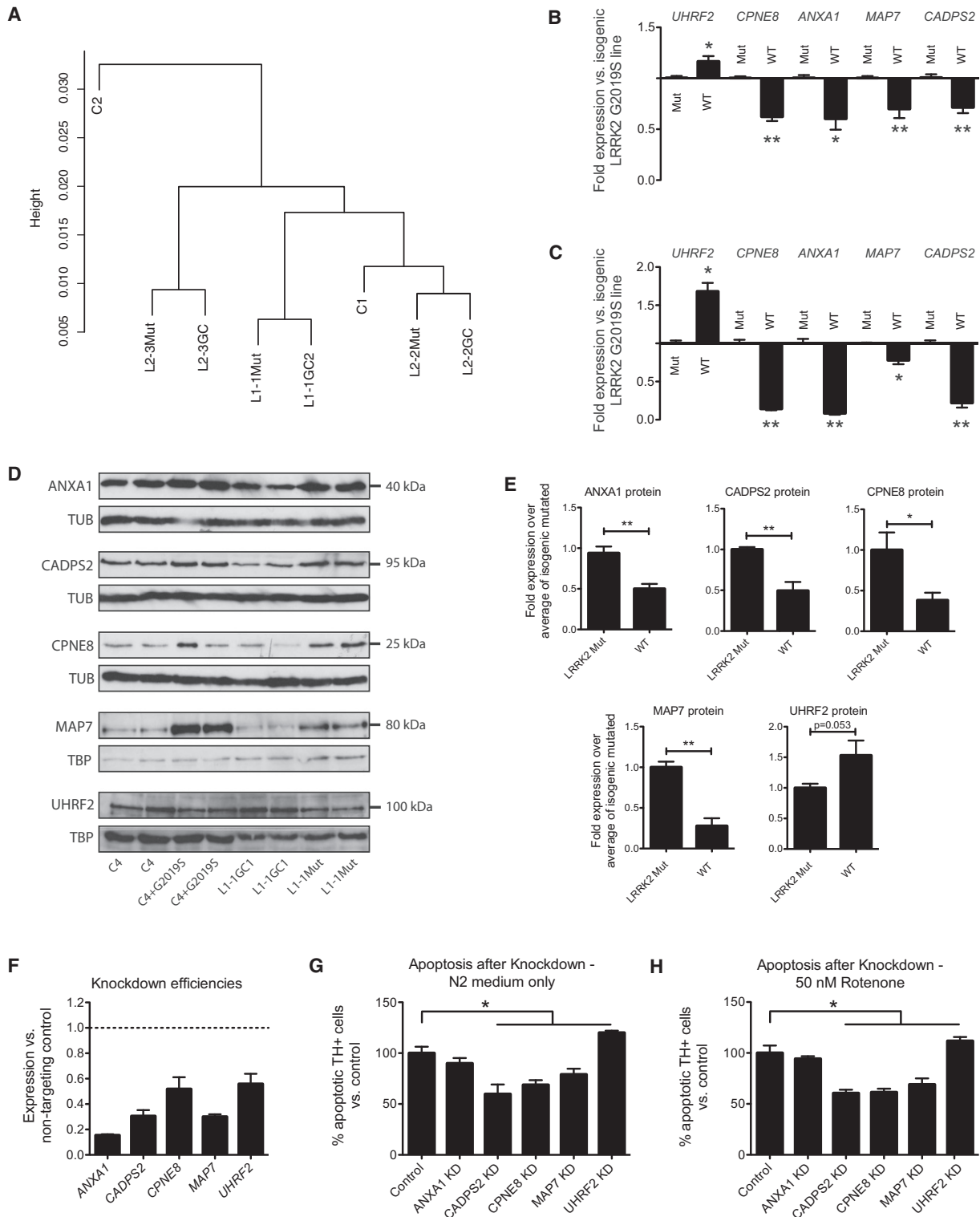


**Figure 6. Identification and Validation of Novel Genes Contributing to PD-Associated Phenotypes Induced by *LRRK2* G2019S**

(A) Cluster analysis of the whole-genome expression profile after 30 days differentiation of the indicated cell lines. Only isogenic iPSC lines give extremely comparable differentiation outcome. Interestingly, C1 clusters closer to L2 and C2 closer to L1, which is opposite to their matches based upon age and gender. (B) Candidate genes dysregulated by *LRRK2* G2019S from the microarray data were validated by qRT-PCR on mDA neuronal cultures differentiated for 30 days in triplicates using isogenic hiPSC lines L1-1Mut with L1-1GC1 and L1-1GC2, L1-2Mut and L1-2GC, L2-2Mut and L2-2GC, L2-3Mut and L2-3GC. (C) hiPSC line C4 and the isogenic line C4+G2019S were differentiated and analyzed by qRT-PCR for the candidate genes. Error bars represent SEM.

(legend continued on next page)

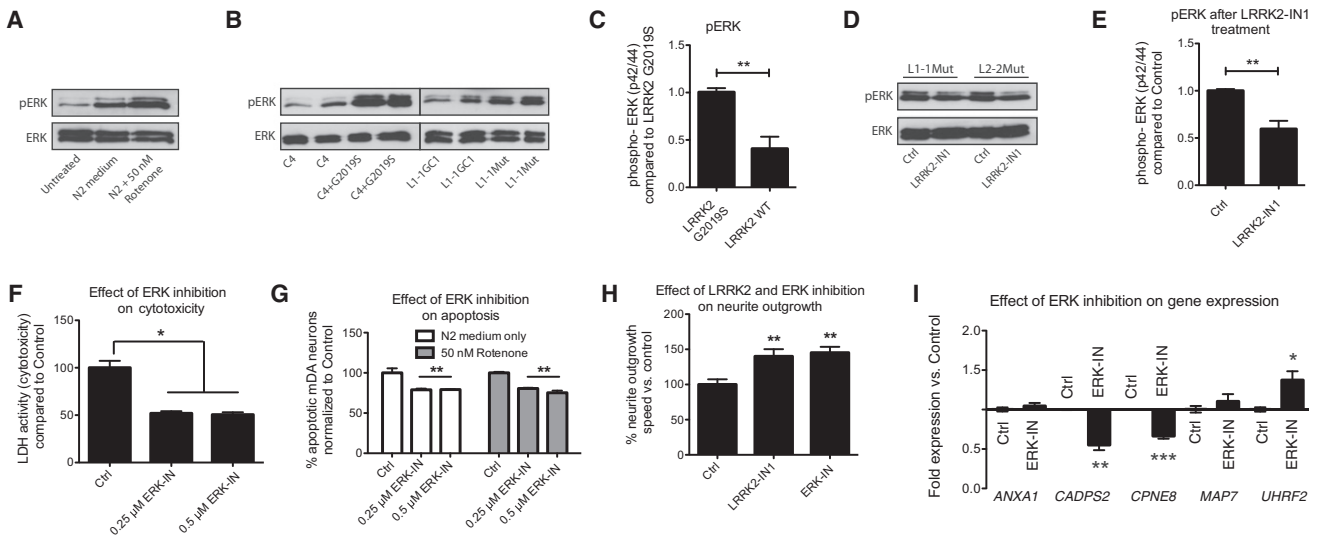


**Figure 7. *LRRK2* G2019S Causes Increased ERK Phosphorylation that Is Responsible for Some of the Observed Phenotypes**

(A) Western blot for phosphorylated ERK1/2 (pERK) and ERK1/2 (ERK) on neurons differentiated for 30 days and cultured under the indicated conditions for 2 days. (B) Representative western blot images of pERK and ERK of mDA neuronal cultured differentiated in duplicate for 30 days from the indicated lines. (C) Quantification of the data from (B) showing significantly increased pERK in cultures harboring *LRRK2* G2019S compared to isogenic controls. (D) Representative western blot for the indicated marker for differentiated cultures from the indicated lines treated for 6 days with 1.5  $\mu$ M LRRK2-IN1 alongside the DMSO-treated control. (E) Quantification of the effect of LRRK2-IN1 on pERK with lines L1-1Mut, L2-2Mut, L2-3Mut, and C4+G2019S in duplicates of treatment, alongside their DMSO-treated controls for 6 days. (F and G) mDA cultures of the line L1-1Mut at day 30 of differentiation were treated for 2 days with PD0325901 (ERK-IN), an ERK phosphorylation-inhibitor, at the given concentrations, which reduced cytotoxicity from stress with 50 nM rotenone as measured by LDH release (F) and cleaved CASPASE3 and TH double-positive cells (G) compared to DMSO-treated controls. (H) Neurite outgrowth assay on neurons differentiated for 30 days and treated with the indicated compounds compared to DMSO-treated controls. (I) qRT-PCR for the indicated genes on neurons differentiated for 30 days and treated with ERK-IN relative to DMSO-treated controls.

\* $p < 0.05$ , \*\* $p < 0.01$ , \*\*\* $p < 0.001$  according to t test. Error bars represent SEM in all panels.

*CADPS2*, and *MAP7* by *LRRK2* G2019S contributes to the mDA neurodegenerative phenotype observed. The small, but significant, increase in mDA degeneration resulting from *UHRF2* knockdown is consistent with the small decrease in *UHRF2* expression observed in cultures with *LRRK2* G2019S. Western blotting after knockdown of *MAP7* reduced  $\alpha$ SYN by about 50% in cultures differentiated from iPSCs harboring *LRRK2* G2019S (Figures S7C and S7D). Knockdown of *CADP2* and *CPNE8* had mildly reduced  $\alpha$ SYN, but knockdown of *UHRF2* and *ANXA1* had no effect (Figures S7C and S7D).

**Higher Sensitivity of *LRRK2* G2019S Neurons to Oxidative Stress Involves the Activation of ERK**

Previously, it was shown that *LRRK2* G2019S causes abnormalities in basal autophagy in fibroblasts through activation of

ERK1/2 (ERK) (Bravo-San Pedro et al., 2013). In addition, neurite shortening by *LRRK2* G2019S has been linked to ERK signaling (Plowey et al., 2008). For these reasons, we performed western blotting to quantify the level of phosphorylated ERK1/2 (pERK), which is the active form of ERK. Cultures of mDA neurons had increased pERK levels after B27 withdrawal compared to controls, and addition of rotenone further increased levels of pERK (Figure 7A). Untreated mDA cultures harboring wild-type *LRRK2* had 50% less pERK compared to isogenic cultures with *LRRK2* G2019S (Figures 7B and 7C). When cultures of mDA neurons were treated with LRRK2-IN1, pERK levels were significantly decreased by more than 40% (Figures 7D and 7E). Treatment with PD0325901 (hereafter ERK-IN), an inhibitor of ERK phosphorylation, rescued cultures of mDA neurons from degeneration and reduced overall

(D) Representative western blot pictures for the newly identified genes from the indicated lines taken at day 30 of duplicate differentiation cultures from the indicated isogenic lines. TBP and  $\alpha$ -TUBULIN (TUB) were used as loading controls.

(E) Densitometric quantification of the western blots from (D). For *ANXA1* and *CADPS2*, duplicate cultures differentiated from L2-2Mut and L2-3Mut were additionally used. Error bars indicate SEM.

(F) Knockdown efficiency was determined by qRT-PCR for the indicated genes normalized to nontargeting controls in mDA neuron cultures differentiated for 30 days from the line L1-1Mut. Error bars show the variance from two parallel cultures.

(G and H) Knockdown of *CADPS2*, *CPNE8*, *MAP7*, and *UHRF2* but not *ANXA1* had a significant effect on the sensitivity of mDA neurons when treated with N2 medium alone (G) or N2 supplemented with 50 nM rotenone (H), as measured by the amount of cleaved CASPASE3 and TH double-positive neurons. Error bars represent SEM.

\* $p < 0.05$  and \*\* $p < 0.01$  according to t test.

cytotoxicity when treated with oxidative stress (Figures 7F and 7G). Finally, ERK-IN and *LRRK2*-IN1 increased neurite outgrowth of differentiated neurons compared to DMSO-treated controls (Figure 7H). Therefore, *LRRK2* G21019S leads to activation of ERK, which contributes to the mDA neurodegenerative phenotype observed in vitro.

We next tested whether activation of ERK contributed to the dysregulation of our newly identified genes. To do this, qRT-PCR was performed on cultures of mDA neurons treated with ERK-IN for 4 days. We observed that expression of *CADPS2*, *CPNE8*, and *UHRF2* was significantly altered by ERK inhibition in the opposite direction compared to that induced by *LRRK2* G2019S (Figure 7I). Taken together, these results suggest that *CADPS2*, *CPNE8*, and *UHRF2* expression is dysregulated by *LRRK2* G2019S through aberrant ERK activation. However, the results for *ANXA1* and *MAP7* suggest that *LRRK2* G2019S might also contribute to PD phenotypes through additional mechanisms.

## DISCUSSION

Reprogramming is a breakthrough technology that enables the generation of patient-specific stem cells. By using patients with PD-causing mutations, such as *LRRK2* G2019S, it is possible to derive iPSCs that recapitulate aspects of PD pathology (Nguyen et al., 2011; Sánchez-Danés et al., 2012). However, because of variance in genetic backgrounds, which is likely to arise from polymorphisms in other genes, each individual might behave differently with respect to a given mutation. Recently, Liu et al. (2012) reported the derivation of iPSCs from PD patients harboring *LRRK2* G2019S as well as isogenic gene-corrected controls. The authors demonstrated phenotypic changes in the nuclear envelope. Although interesting, these changes lack a clear causal link to PD pathogenesis. In addition, the authors studied primitive neural stem cells, which are most closely related to cells present in early post-implantation-stage embryos that are not present in fetuses, neonates, or adults (Hitoshi et al., 2004; Liu et al., 2012). Therefore, there is still significant potential for gene-corrected iPSCs to elucidate the molecular mechanisms underlying PD pathogenesis in mDA neurons.

Here, we have demonstrated that neurons differentiated from iPSCs derived from patients with PD harboring *LRRK2* G2019S exhibit multiple phenotypes including reduced neurite outgrowth and increased sensitivity to stress. By using gene-corrected isogenic cultures and the introduction of the mutation into a control iPSC line, we show that these phenotypes were specifically associated with *LRRK2* G2019S. Because an inhibitor of *LRRK2* kinase activity ameliorated these phenotypes, the G2019S mutation probably results in increased kinase activity, which is consistent with previous reports (Gloeckner et al., 2006; West et al., 2005).

Gene correction enabled the discovery of genes that contribute to PD-associated phenotypes in cultured mDA neurons induced by *LRRK2* G2019S. Expression profiling of multiple pairs of isogenic cultures resulted in the identification of a handful of genes that were consistently dysregulated by *LRRK2* G2019S including *CPNE8*, *CADPS2*, *MAP7*, and *UHRF2*. Western blotting confirmed differences in the level of protein, and siRNA

experiments demonstrated that this dysregulation contributed to mDA degeneration.

Interestingly, these genes have previously been implicated in neurodegenerative phenotypes in multiple ways. Polymorphisms in *CPNE8* have been shown to affect the incubation time of prion disease in mice (Lloyd et al., 2010). Interestingly, PD has been proposed to be a prion-like disease involving  $\alpha$ SYN (Polymenidou and Cleveland, 2012). We could confirm previous reports of increased levels of  $\alpha$ SYN with mutant *LRRK2* (Nguyen et al., 2011; Sánchez-Danés et al., 2012). It is possible that the reported defects in autophagy induced by *LRRK2* G2019S contribute to the increased level of  $\alpha$ SYN protein because there is no detectable increase in *SNCA* transcription.

*UHRF2* is an E3 ubiquitin ligase with the same catalytic activity as *PARKIN*. Because loss-of-function mutations in *PARKIN* cause PD, the downregulation of *UHRF2* in cultures of mDA neurons containing the PD-associated mutation *LRRK2* G2019S is significant. In addition, *UHRF2* has previously been shown to enhance clearance of polyglutamine aggregates, which cause neurodegeneration in several diseases (Iwata et al., 2009). It is tempting to speculate that *UHRF2* could play a similar role for  $\alpha$ SYN. Consequently, the increased levels of *CPNE8* and  $\alpha$ SYN and decreased levels of *UHRF2* proteins suggest that *LRRK2* G2019S could act on multiple mechanisms to increase the initiation of synucleinopathy.

*CADPS2* dysregulation also has potentially significant implications for mDA neurodegeneration. The protein *CADPS2* has been demonstrated to regulate the neurotransmission of monoamines, of which dopamine is an example (Brunk et al., 2009). This is of interest because transgenic mice overexpressing *LRRK2* variants show dysregulation of dopamine release (Li et al., 2010). Dopamine is thought to increase oxidative stress in mDA neurons through the formation of reactive metabolites (Napolitano et al., 2011). Consequently, dysregulation of *CADPS2* by *LRRK2* G2019S could result in aberrant formation of toxic metabolites. Consistent with this idea, increased oxidative stress, for example by administration of rotenone, is known to induce PD-like pathogenesis and induced mDA-specific neurodegeneration in vitro in our differentiated hiPSC cultures (Inden et al., 2011).

Because *LRRK2* is not a transcription factor, additional proteins probably mediate the transcriptional dysregulation we observed. We have shown that *LRRK2* G2019S resulted in increased phosphorylation of ERK in cultures of human mDA neurons. Inhibition of ERK activity rescued mDA neurons in our system, which suggests that ERK activity is crucial for the pathogenesis of mutant *LRRK2*. Two previously published reports could account for the link of *LRRK2* with ERK. First, Ste20 family kinases, which are upstream of ERK and are induced by stress, are phosphorylated by *LRRK2* protein (Zach et al., 2010). Second, it has been shown that Endophilin A1 is directly phosphorylated by *LRRK2* (Matta et al., 2012). Consistent with this finding, knockdown of Endophilin A1 resulted in decreased ERK activation by BDNF (Fu et al., 2011). It is also significant to note that the autophagy defect caused by *LRRK2* has also been linked to ERK activity (Bravo-San Pedro et al., 2013). Taken together, our results suggest possible targets for the development of new therapeutics for patients with PD.

## EXPERIMENTAL PROCEDURES

## Generation of Induced Pluripotent Stem Cells

Informed consent was obtained from all patients involved in our study prior to cell donation. The Ethics Committee of the Medical Faculty and the University Hospital Tübingen previously approved this consent form. Dermal fibroblasts, obtained from skin biopsies of patients with PD and healthy controls, were cultured. Reprogramming was adapted from Takahashi et al. (2007). Human iPSCs were cultured on mitomycin C (Tocris)-inactivated MEFs. Gene correction was performed by nucleofection of ZFN constructs targeting *LRRK2* (Sigma). 50 µg/ml G418 (PAA) 2 µM ganciclovir (Sigma)-resistant colonies were picked and clonally expanded on MEFs.

## iPSC Differentiation into mDA Neurons

mDA neurons were generated via adapted protocol (Chambers et al., 2009; Nguyen et al., 2011). Confluent iPSCs were cultured with 1 µM dorsomorphin (Tocris), 10 µM SB431542, and 0.5 µM purmorphamine (PMA, Alexis). mDA patterning was performed with N2 medium supplemented with 0.5 µM PMA, 100 ng/ml human FGF8, 20 ng/ml human BDNF (both Peprotech), and 200 µM ascorbic acid (AA, Sigma). Maturation was induced by culturing with BDNF, AA, GDNF, TGF-β, and dbcAMP. mDA neuron differentiation cultures were replated as single cells on about day 30 on Matrigel-coated 48-well plates.

## Protein Analysis

Cell pellets of differentiated neurons were extracted with RIPA-Buffer containing protease inhibitors (Mini complete, Roche) on ice. Supernatant were mixed with 6× Laemmli buffer. 15 µg of the protein lysate were loaded on a 4%–12% gel (NuPAGE, Invitrogen) after incubation at 95°C for 5 min and then blotted on a PVDF membrane. The membrane was blocked and incubated with the indicated primary antibodies (listed in Supplemental Information). After 3× washing, the blot was incubated with HRP coupled secondary antibody. The membrane was washed and then developed with chemiluminescent HRP substrate solution (Millipore, GE). Protein bands were standardized on GAPDH, TBP, β-actin, or α-TUBULIN.

## Quantification of the Cytotoxicity of 6-OHDA and Rotenone

mDA neuron differentiation cultures on days 27–35 were disaggregated and plated as single cells. 2 days later, cultures were fed with N2 medium without supplements for 6 hr. This medium was replaced with warm N2 medium supplemented with 10 µM 6-OHDA, 2 µM 6-OHDA, 50 nM rotenone, or 100 nM rotenone and incubated for 48 hr. Afterwards, the cell cultures were fixed and stained.

## Quantitative RT-PCR

Total RNA was isolated from cell culture samples with RNeasy columns (QIAGEN) including on-column DNA digestion. cDNA was prepared with oligo-dT16 primers (Metabion) and M-MLV reverse transcriptase (USB). Cycling was carried out on an ABI 7300 Real-Time PCR system. Relative expression levels were calculated via the  $2^{-2\Delta\Delta C_T}$  method, based on biological reference samples and housekeeping genes for normalization. Primer sequences are listed in Table S2.

## Whole-Genome Expression Analysis

DNA-free total RNA samples (500 ng) to be hybridized on Illumina human-12 V3 expression BeadChips were processed with a linear amplification kit (Ambion) generating biotin-labeled cRNA (IVT duration: 14 hr). Raw data were background subtracted and normalized via the “cubic spline” algorithm. Data analysis was done with MS Excel and R (Bioconductor, pvcust).

## Gene Knockdown

Self-transfecting Accell siRNA (nontargeting green fluorescent control, *ANXA1*, *CADPS2*, *CPNE8*, *MAP7*, *UHRF2*; Thermo) SMARTPool are mixtures of four siRNAs targeting a single gene. siRNA was diluted in maturation medium and added to the cells twice every other day (for RNA extraction). For the cytotoxicity experiments, siRNA was added starting 2 days before reseeded, during reseeded, and 2 days later during the stressing procedure.

## Inhibitor Treatment

For RNA and protein sample isolation, mDA neuron cultures were treated with maturation medium supplemented with 1.5 µM *LRRK2*-IN1 for 6 days and 0.5 µM PD0325901 (both Merck) for 2–4 days and compared to DMSO alone. Medium was changed every other day. For determining neural survival, cultures were treated starting 2 days before reseeded.

## ACCESSION NUMBERS

The data have been deposited in GEO at NCBI under the accession number GSE43364.

## SUPPLEMENTAL INFORMATION

Supplemental Information includes Supplemental Experimental Procedures, seven figures, and two tables and can be found with this article online at <http://dx.doi.org/10.1016/j.stem.2013.01.008>.

## ACKNOWLEDGMENTS

This work was supported by grants from the German Research (WO 1610/2-1 to M.M. and T.G.; KR2119/8-1 to R.K. and T.G.); Fortuene (Nr. 1831-0-0-0-0 to M.M.); the German Research Council (DFG, KR2119/8-1 to R.K. and T.G.); Fritz Thyssen Foundation (10.11.2.153 to R.K.); the Michael J. Fox Foundation (LRRK2 Biology LEAPS Award, 2012); and by a doctoral scholarship from the charitable Hertie Foundation (to L.F.B.). Plasmids for reprogramming were obtained from Addgene: Addgene plasmids 8449, 8454, 17217, 17218, 17219, and 17220. We would like to acknowledge Ann-Kathrin Hauser for the sequencing analysis. We would like to thank Kerstin Hergarten and Rhea Brintrup for excellent technical support.

Received: August 21, 2012

Revised: December 6, 2012

Accepted: January 11, 2013

Published: March 7, 2013

## REFERENCES

- Badiola, N., de Oliveira, R.M., Herrera, F., Guardia-Laguarta, C., Gonçalves, S.A., Pera, M., Suárez-Calvet, M., Clarimon, J., Outeiro, T.F., and Lleó, A. (2011). Tau enhances α-synuclein aggregation and toxicity in cellular models of synucleinopathy. *PLoS ONE* 6, e26609.
- Berg, D., Schweitzer, K.J., Leitner, P., Zimprich, A., Lichtner, P., Belcredi, P., Brüsel, T., Schulte, C., Maass, S., Nägele, T., et al. (2005). Type and frequency of mutations in the *LRRK2* gene in familial and sporadic Parkinson's disease. *Brain* 128, 3000–3011.
- Botta-Orfila, T., Ezquerro, M., Pastor, P., Fernández-Santiago, R., Pont-Sunyer, C., Compta, Y., Lorenzo-Betancor, O., Samaranch, L., Martí, M.J., Valldeoriola, F., et al. (2012). Age at onset in *LRRK2*-associated PD is modified by SNCA variants. *J. Mol. Neurosci.* 48, 245–247.
- Bravo-San Pedro, J.M., Niso-Santano, M., Gomez-Sanchez, R., Pizarro-Estrella, E., Aiastui-Pujana, A., Gorostidi, A., Climent, V., Lopez de Maturana, R., Sanchez-Pernate, R., Lopez de Munain, A., et al. (2013). The *LRRK2* G2019S mutant exacerbates basal autophagy through activation of the MEK/ERK pathway. *Cell. Mol. Life Sci.* 70, 121–136.
- Brewer, G.J., Torricelli, J.R., Evege, E.K., and Price, P.J. (1993). Optimized survival of hippocampal neurons in B27-supplemented Neurobasal, a new serum-free medium combination. *J. Neurosci. Res.* 35, 567–576.
- Brunk, I., Blex, C., Speidel, D., Brose, N., and Ahnert-Hilger, G. (2009). Ca<sup>2+</sup>-dependent activator proteins of secretion promote vesicular monoamine uptake. *J. Biol. Chem.* 284, 1050–1056.
- Carballo-Carbajal, I., Weber-Endress, S., Rovelli, G., Chan, D., Wolozin, B., Klein, C.L., Patenge, N., Gasser, T., and Kahle, P.J. (2010). Leucine-rich repeat kinase 2 induces alpha-synuclein expression via the extracellular signal-regulated kinase pathway. *Cell. Signal.* 22, 821–827.

- Chambers, S.M., Fasano, C.A., Papapetrou, E.P., Tomishima, M., Sadelain, M., and Studer, L. (2009). Highly efficient neural conversion of human ES and iPS cells by dual inhibition of SMAD signaling. *Nat. Biotechnol.* *27*, 275–280.
- Cookson, M.R. (2010). The role of leucine-rich repeat kinase 2 (LRRK2) in Parkinson's disease. *Nat. Rev. Neurosci.* *11*, 791–797.
- Cookson, M.R., Hardy, J., and Lewis, P.A. (2008). Genetic neuropathology of Parkinson's disease. *Int. J. Clin. Exp. Pathol.* *1*, 217–231.
- European Brain Council (2011). Parkinson's disease Fact Sheet. <http://www.europeanbraincouncil.org/pdfs/Documents/Parkinson%27s%20fact%20sheet%20July%202011.pdf>.
- Fu, X., Yang, Y., Xu, C., Niu, Y., Chen, T., Zhou, Q., and Liu, J.J. (2011). Retrolinkin cooperates with endophilin A1 to mediate BDNF-TrkB early endocytic trafficking and signaling from early endosomes. *Mol. Biol. Cell* *22*, 3684–3698.
- Gloeckner, C.J., Kinkl, N., Schumacher, A., Braun, R.J., O'Neill, E., Meitinger, T., Kolch, W., Prokisch, H., and Ueffing, M. (2006). The Parkinson disease causing LRRK2 mutation I2020T is associated with increased kinase activity. *Hum. Mol. Genet.* *15*, 223–232.
- Golub, Y., Berg, D., Calne, D.B., Pfeiffer, R.F., Uitti, R.J., Stoessl, A.J., Wszolek, Z.K., Farrer, M.J., Mueller, J.C., Gasser, T., and Fuchs, J. (2009). Genetic factors influencing age at onset in LRRK2-linked Parkinson disease. *Parkinsonism Relat. Disord.* *15*, 539–541.
- Greber, B., Coulon, P., Zhang, M., Moritz, S., Frank, S., Müller-Molina, A.J., Araúzo-Bravo, M.J., Han, D.W., Pape, H.C., and Schöler, H.R. (2011). FGF signalling inhibits neural induction in human embryonic stem cells. *EMBO J.* *30*, 4874–4884.
- Hitoshi, S., Seaberg, R.M., Kosciak, C., Alexson, T., Kusunoki, S., Kanazawa, I., Tsuji, S., and van der Kooy, D. (2004). Primitive neural stem cells from the mammalian epiblast differentiate to definitive neural stem cells under the control of Notch signaling. *Genes Dev.* *18*, 1806–1811.
- Hotta, A., and Ellis, J. (2008). Retroviral vector silencing during iPS cell induction: an epigenetic beacon that signals distinct pluripotent states. *J. Cell. Biochem.* *105*, 940–948.
- Inden, M., Kitamura, Y., Abe, M., Tamaki, A., Takata, K., and Taniguchi, T. (2011). Parkinsonian rotenone mouse model: reevaluation of long-term administration of rotenone in C57BL/6 mice. *Biol. Pharm. Bull.* *34*, 92–96.
- Ishizawa, T., Mattila, P., Davies, P., Wang, D., and Dickson, D.W. (2003). Colocalization of tau and alpha-synuclein epitopes in Lewy bodies. *J. Neuropathol. Exp. Neurol.* *62*, 389–397.
- Iwata, A., Nagashima, Y., Matsumoto, L., Suzuki, T., Yamanaka, T., Date, H., Deoka, K., Nukina, N., and Tsuji, S. (2009). Intracellular degradation of polyglutamine aggregates by the ubiquitin-proteasome system. *J. Biol. Chem.* *284*, 9796–9803.
- Li, X., Patel, J.C., Wang, J., Avshalomov, M.V., Nicholson, C., Buxbaum, J.D., Elder, G.A., Rice, M.E., and Yue, Z. (2010). Enhanced striatal dopamine transmission and motor performance with LRRK2 overexpression in mice is eliminated by familial Parkinson's disease mutation G2019S. *J. Neurosci.* *30*, 1788–1797.
- Lin, X., Parisiadou, L., Gu, X.L., Wang, L., Shim, H., Sun, L., Xie, C., Long, C.X., Yang, W.J., Ding, J., et al. (2009). Leucine-rich repeat kinase 2 regulates the progression of neuropathology induced by Parkinson's-disease-related mutant alpha-synuclein. *Neuron* *64*, 807–827.
- Liu, G.H., Qu, J., Suzuki, K., Nivet, E., Li, M., Montserrat, N., Yi, F., Xu, X., Ruiz, S., Zhang, W., et al. (2012). Progressive degeneration of human neural stem cells caused by pathogenic LRRK2. *Nature* *491*, 603–607.
- Lloyd, S.E., Maytham, E.G., Grizenkova, J., Hummerich, H., and Collinge, J. (2010). A Copine family member, *Cpne8*, is a candidate quantitative trait gene for prion disease incubation time in mouse. *Neurogenetics* *11*, 185–191.
- MacLeod, D., Dowman, J., Hammond, R., Leete, T., Inoue, K., and Abeliovich, A. (2006). The familial Parkinsonism gene LRRK2 regulates neurite process morphology. *Neuron* *52*, 587–593.
- Maldonado, H., Ortiz-Riaño, E., Krause, B., Barriga, A., Medina, F., Pando, M.E., Alberti, C., Kettlun, A.M., Collados, L., García, L., et al. (2008). Microtubule proteins and their post-translational forms in the cerebrospinal fluid of patients with paraparesis associated with HTLV-I infection and in SH-SY5Y cells: an in vitro model of HTLV-I-induced disease. *Biol. Res.* *41*, 239–259.
- Maldonado, H., Ramírez, E., Utreras, E., Pando, M.E., Kettlun, A.M., Chiong, M., Kulkarni, A.B., Collados, L., Puente, J., Cartier, L., and Valenzuela, M.A. (2011). Inhibition of cyclin-dependent kinase 5 but not of glycogen synthase kinase 3- $\beta$  prevents neurite retraction and tau hyperphosphorylation caused by secretable products of human T-cell leukemia virus type I-infected lymphocytes. *J. Neurosci. Res.* *89*, 1489–1498.
- Matta, S., Van Kolen, K., da Cunha, R., van den Bogaart, G., Mandemakers, W., Miskiewicz, K., De Bock, P.J., Morais, V.A., Vilain, S., Haddad, D., et al. (2012). LRRK2 controls an EndoA phosphorylation cycle in synaptic endocytosis. *Neuron* *75*, 1008–1021.
- Napolitano, A., Manini, P., and d'Ischia, M. (2011). Oxidation chemistry of catecholamines and neuronal degeneration: an update. *Curr. Med. Chem.* *18*, 1832–1845.
- Nguyen, H.N., Byers, B., Cord, B., Shcheglovitov, A., Byrne, J., Gujar, P., Kee, K., Schüle, B., Dolmetsch, R.E., Langston, W., et al. (2011). LRRK2 mutant iPSC-derived DA neurons demonstrate increased susceptibility to oxidative stress. *Cell Stem Cell* *8*, 267–280.
- Ozelius, L.J., Senthil, G., Saunders-Pullman, R., Ohmann, E., Deligtisch, A., Tagliati, M., Hunt, A.L., Klein, C., Henick, B., Hailpern, S.M., et al. (2006). LRRK2 G2019S as a cause of Parkinson's disease in Ashkenazi Jews. *N. Engl. J. Med.* *354*, 424–425.
- Paisán-Ruiz, C., Jain, S., Evans, E.W., Gilks, W.P., Simón, J., van der Brug, M., López de Munain, A., Aparicio, S., Gil, A.M., Khan, N., et al. (2004). Cloning of the gene containing mutations that cause PARK8-linked Parkinson's disease. *Neuron* *44*, 595–600.
- Plowey, E.D., Cherra, S.J., 3rd, Liu, Y.J., and Chu, C.T. (2008). Role of autophagy in G2019S-LRRK2-associated neurite shortening in differentiated SH-SY5Y cells. *J. Neurochem.* *105*, 1048–1056.
- Polymenidou, M., and Cleveland, D.W. (2012). Prion-like spread of protein aggregates in neurodegeneration. *J. Exp. Med.* *209*, 889–893.
- Polymeropoulos, M.H., Lavedan, C., Leroy, E., Ide, S.E., Dehejia, A., Dutra, A., Pike, B., Root, H., Rubenstein, J., Boyer, R., et al. (1997). Mutation in the alpha-synuclein gene identified in families with Parkinson's disease. *Science* *276*, 2045–2047.
- Rajput, A., Dickson, D.W., Robinson, C.A., Ross, O.A., Dächsel, J.C., Lincoln, S.J., Cobb, S.A., Rajput, M.L., and Farrer, M.J. (2006). Parkinsonism, *Lrrk2* G2019S, and tau neuropathology. *Neurology* *67*, 1506–1508.
- Ross, O.A., Toft, M., Whittle, A.J., Johnson, J.L., Papapetropoulos, S., Mash, D.C., Litvan, I., Gordon, M.F., Wszolek, Z.K., Farrer, M.J., and Dickson, D.W. (2006). *Lrrk2* and Lewy body disease. *Ann. Neurol.* *59*, 388–393.
- Sánchez-Danés, A., Richaud-Patin, Y., Carballo-Carbajal, I., Jiménez-Delgado, S., Caig, C., Mora, S., Di Guglielmo, C., Ezquerro, M., Patel, B., Giralt, A., et al. (2012). Disease-specific phenotypes in dopamine neurons from human iPSC-based models of genetic and sporadic Parkinson's disease. *EMBO Mol. Med.* *4*, 380–395.
- Schiesling, C., Kieper, N., Seidel, K., and Krüger, R. (2008). Review: Familial Parkinson's disease—genetics, clinical phenotype and neuropathology in relation to the common sporadic form of the disease. *Neuropathol. Appl. Neurobiol.* *34*, 255–271.
- Simón-Sánchez, J., Schulte, C., Bras, J.M., Sharma, M., Gibbs, J.R., Berg, D., Paisán-Ruiz, C., Lichtner, P., Scholz, S.W., Hernandez, D.G., et al. (2009). Genome-wide association study reveals genetic risk underlying Parkinson's disease. *Nat. Genet.* *41*, 1308–1312.
- Spillantini, M.G., Schmidt, M.L., Lee, V.M., Trojanowski, J.Q., Jakes, R., and Goedert, M. (1997). Alpha-synuclein in Lewy bodies. *Nature* *388*, 839–840.

Takahashi, K., and Yamanaka, S. (2006). Induction of pluripotent stem cells from mouse embryonic and adult fibroblast cultures by defined factors. *Cell* 126, 663–676.

Takahashi, K., Tanabe, K., Ohnuki, M., Narita, M., Ichisaka, T., Tomoda, K., and Yamanaka, S. (2007). Induction of pluripotent stem cells from adult human fibroblasts by defined factors. *Cell* 131, 861–872.

West, A.B., Moore, D.J., Biskup, S., Bugayenko, A., Smith, W.W., Ross, C.A., Dawson, V.L., and Dawson, T.M. (2005). Parkinson's disease-associated

mutations in leucine-rich repeat kinase 2 augment kinase activity. *Proc. Natl. Acad. Sci. USA* 102, 16842–16847.

Zach, S., Felk, S., and Gillardon, F. (2010). Signal transduction protein array analysis links LRRK2 to Ste20 kinases and PKC zeta that modulate neuronal plasticity. *PLoS ONE* 5, e13191.

Zimprich, A., Biskup, S., Leitner, P., Lichtner, P., Farrer, M., Lincoln, S., Kachergus, J., Hulihan, M., Uitti, R.J., Calne, D.B., et al. (2004). Mutations in LRRK2 cause autosomal-dominant parkinsonism with pleomorphic pathology. *Neuron* 44, 601–607.